Morphology Control of Nanoscale PbS Particles in a Polyol Process

Zeping Peng,[†,‡] Yusheng Jiang,[†] Yonghai Song,[‡] Cheng Wang,*[,†] and Hongjie Zhang*[,†]

State Key Laboratory of Rare Earth Resources Utilization, Changchun Institute of Applied Chemistry, and Graduate School of the Chinese Academy of Sciences, Changchun 130022, People's Republic of China

Received December 31, 2007. Revised Manuscript Received February 16, 2008

Nanostructured PbS with different morphologies and particle sizes have been prepared through a polyol process. Narrow size distribution for star-shaped, octahedral, tetradecanehedral, and cubic products were achieved by slowly introducing the source materials using a peristaltic pump in the presence of poly(vinylpyrrolidone) (PVP) as additive. Systematic variation of the kinetic factors, including the additive, the reaction temperature, the duration time, the ratio of source materials, the sulfur sources, and the $Pb(Ac)_2 \cdot 3H_2O$ concentration, reveals that the morphology depends mainly on the supersaturation degree of the free sulfur ions released from thiourea under elevated temperature. Semiquantitative analysis based on the X-ray diffraction (XRD) patterns of these products gives that the peak area ratio of (200) to (111) increases with the increase of the supersaturation degree within the reaction system. The four types of symmetric morphology showed different oxidation stability toward the 514.5 nm argon ion laser irradiation when the power was set at 12.5 mW.

Introduction

The development of solution-based chemical control synthesis of nanostructured materials has experienced from monodispersed particles to one-dimensional (1D) nanowires or nanorods, multipods, and polygons over the past 2 decades. Following the pioneer theoretical study of semiconductor nanocrystallites by Brus,[1] tremendous efforts have been made to synthesize monodispersed nanocrystallites with quantum size effects.[2–8] Using a simple effective-mass approximation,[9,10] it has been demonstrated that the optical properties of nonspherical semiconductor nanocrystals are mainly controlled by the lowest dimension of the nanocrystals, and the carriers for 1D nanostructures are also confined in one dimension. Therefore many efforts have been made for the synthesis of anisotropic nanostructures, especially 1D semiconductors, in liquid media through hydro(solvo)thermal and high-temperature refluxing processes[11–15] besides physical or/and chemical vapor deposition approaches to carbon nanotubes[16] and 1D III−V semiconductors.[10–12] Multipods of nanocrystalline metals,[17–19] metal oxides,[20,21] and chalcogenides[22–29] have been fabricated through delicately manipulating the kinetic factors, in most cases, in synthetic systems similar for 1D nanostructures. As an extension of this trend, recently, many symmetric polygonal nanocrystals or sub-micrometer crystals of noble metals,[30–34] Cu_2O,[35,36] Cu_4S_7,[37] PbSe,[38] and PbTe[39,40] have been syntheiszed.

* To whom correspondence should be addressed. E-mail: cwang@ciac.jl.cn (C.W.); hongjie@ciac.jl.cn (H.Z.).

† State Key Laboratory of Rare Earth Resources Utilization, Changchun Institute of Applied Chemistry.

‡ Graduate School of the Chinese Academy of Sciences.

(1) Brus, L. E. *J. Chem. Phys.* **1984**, *80*, 4403–4409.
(2) Kortan, A. R.; Hull, R.; Opila, R. L.; Bawendi, M. G.; Steigerwald, M. L.; Carroll, P. J.; Brus, L. E. *J. Am. Chem. Soc.* **1990**, *112*, 1327–1332.
(3) Wang, Y.; Herron, N. *J. Phys. Chem.* **1991**, *95*, 525–532.
(4) Murray, C. B.; Norris, D. J.; Bawendi, M. G. *J. Am. Chem. Soc.* **1993**, *115*, 8706–8715.
(5) Peng, X. G.; Wickham, J.; Alivisatos, A. P. *J. Am. Chem. Soc.* **1998**, *120*, 5343–5344.
(6) Peng, Z. A.; Peng, X. G. *J. Am. Chem. Soc.* **2001**, *123*, 183–184.
(7) Wang, X.; Zhuang, J.; Peng, Q.; Li, Y. D. *Nature* **2005**, *437*, 121–124.
(8) Cao, Y. C.; Wang, J. H. *J. Am. Chem. Soc.* **2004**, *126*, 14336–14337.
(9) Collins, R. T.; Fauchet, P. M.; Tischler, M. A. *Phys. Today* **1997**, *50*, 24–31.
(10) Nanda, K. K.; Sahu, S. N. *Adv. Mater.* **2001**, *13*, 280+.
(11) Li, Y. D.; Liao, H. W.; Ding, Y.; Qian, Y. T.; Yang, L.; Zhou, G. E. *Chem. Mater.* **1998**, *10*, 2301–2303.
(12) Peng, X.; Manna, L.; Yang, W.; Wickham, J.; Scher, E.; Kadavanich, A.; Alivisatos, A. P. *Nature* **2000**, *404*, 59–61.
(13) Peng, Z. A.; Peng, X. G. *J. Am. Chem. Soc.* **2002**, *124*, 3343–3353.
(14) Li, R. F.; Luo, Z. T.; Papadimitrakopoulos, F. *J. Am. Chem. Soc.* **2006**, *128*, 6280–6281.
(15) Halpert, J. E.; Porter, V. J.; Zimmer, J. P.; Bawendi, M. G. *J. Am. Chem. Soc.* **2006**, *128*, 12590–12591.
(16) Iijima, S. *Nature* **1991**, *354*, 56–58.
(17) Teng, X.; Yang, H. *Nano Lett.* **2005**, *5*, 885–891.
(18) Zettsu, N.; McLellan, J. M.; Wiley, B.; Yin, Y.; Li, Z. Y.; Xia, Y. *Angew. Chem., Int. Ed.* **2006**, *45*, 1288.
(19) Hoefelmeyer, J. D.; Niesz, K.; Somorjai, G. A.; Tilley, T. D. *Nano Lett.* **2005**, *5*, 435–438.
(20) Zitoun, D.; Pinna, N.; Frolet, N.; Belin, C. *J. Am. Chem. Soc.* **2005**, *127*, 15034–15035.
(21) Ould-Ely, T.; Prieto-Centurion, D.; Kumar, A.; Guo, W.; Knowles, W. V.; Asokan, S.; Wong, M. S.; Rusakova, I.; Luttge, A.; Whitmire, K. H. *Chem. Mater.* **2006**, *18*, 1821–1829.
(22) Jun, Y. W.; Lee, S. M.; Kang, N. J.; Cheon, J. *J. Am. Chem. Soc.* **2001**, *123*, 5150–5151.
(23) Xu, L.; Zhang, W.; Ding, Y.; Yu, W.; Xing, J.; Li, F.; Qian, Y. *J. Cryst. Growth* **2004**, *273*, 213–219.
(24) Lee, S. M.; Jun, Y. W.; Cho, S. N.; Cheon, J. *J. Am. Chem. Soc.* **2002**, *124*, 11244–11245.
(25) Manna, L.; Scher, E. C.; Alivisatos, A. P. *J. Am. Chem. Soc.* **2000**, *122*, 12700–12706.
(26) Manna, L.; Milliron, D. J.; Meisel, A.; Scher, E. C.; Alivisatos, A. P. *Nat. Mater.* **2003**, *2*, 382–385.
(27) Yong, K. T.; Sahoo, Y.; Swihart, M. T.; Prasad, P. N. *Adv. Mater.* **2006**, *18*, 1978.
(28) Lifshitz, E.; Bashouti, M.; Kloper, V.; Kigel, A.; Eisen, M. S.; Berger, S. *Nano Lett.* **2003**, *3*, 857–862.
(29) Milliron, D. J.; Hughes, S. M.; Cui, Y.; Manna, L.; Li, J. B.; Wang, L. W.; Alivisatos, A. P. *Nature* **2004**, *430*, 190–195.
(30) Wang, Z. L.; Harfenist, S. A.; Vezmar, I.; Whetten, R. L.; Bentley, J.; Evans, N. D.; Alexander, K. B. *Adv. Mater.* **1998**, *10*, 808–812.
(31) Sun, Y. G.; Xia, Y. N. *Science* **2002**, *298*, 2176–2179.

10.1021/cm703707v CCC: $40.75
Published on Web 04/12/2008

Table 1. Experimental Details for Different PbS Morphologies

PbS morphology	PVP[a] (mol/L)	S/Pb[b]	*T* (°C)	duration time (min)
star-shaped	1.0	0.5	110	8
octahedral	1.0	0.5	160	8
tetradecahedral	2.0	1.0	160	8
cube	2.0	1.25	160	8

[a] The concentration of PVP-K30 in 6.0 mL of EG. [b] Mole ratio of thiourea to $Pb(Ac)_2$. The concentration of $Pb(Ac)_2$ in 2.0 mL of EG was fixed at 0.5 mol/L, while the concentration of thiourea in 2.0 mL of EG varied according to the ratio listed in the table.

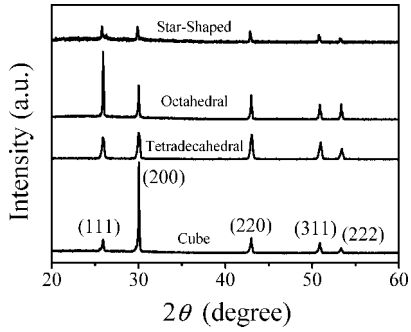

Figure 1. XRD pattern of nanostructured lead sulfides for four typical morphologies.

Table 2. Peak Area of (200) and (111) Planes and Their Ratio

PbS morphology	peak area ratio (200)/(111)	PbS morphology	peak area ratio (200)/(111)
star-shaped	0.96	tetradecahedral	1.14
octahedral	0.69	cube	2.69

Similar to traditional crystal growth, both nucleation and growth get involved during the preparation of nanostructured materials. To obtain small particles with narrow size distributions, homogeneous nucleation is preferred and post-grain growth after initialized nucleation should be impeded. To meet the requirements of homogeneous nucleation, generally, the reaction should be carried out at higher temperature to surmount the energy barrier, and the source materials should reach supersaturation with high level. Using protective agents or stopping the reactions at a certain stage could effectively prevent the post-grain growth from Ostwald ripening.[7,8,27,41–45] Nanocrystals tend to be enclosed by high reticular density planes according to the Bravis rule, if only crystal structure is taken into consideration, as their surface tension is lower and growth on such planes is not favored. However, some high-energy planes should coexist due to incomplete evolution for those extreme small particles. This might explain why small nanoparticles are usually spherical or irregular. In the cases of anisotropic nanostructures, the resulting morphology is a compromise between the intrinsic crystal structure of the material and the kinetic factors employed during the synthetic course. The preferred growth on certain planes becomes energetically favorable only when the surface tensions of these planes are high and the bulk energy of the total system tends to decrease.[41] The surface tensions of these planes could be tuned to allow anisotropic growth through manipulating experimental conditions, such as pH, impurities or additives, and temperature, which have been widely implemented in the synthesis of 1D nanowires as well as multipods and polygonal nanostructures. In such an anisotropic growing process, synthetic strategies should differ from those deployed for monodispersed nanoparticles. Generally, the source materials could be integrated into an existing embryo via three ways: (a) heterogeneous nucleation of the constituents on the existing embryo, (b) Ostwald ripening, and (c) direct oriented attachment of preformed particles.

A polyol process, with most mainly focused on the use of ethylene glycol (EG) as the reaction medium, has been utilized in the synthesis of monodispersed metal powders for more than 2 decades. The polyol plays two key roles in such processes. One is to serve as the solvent for the starting chemicals due to their rather high dielectric constants and boiling points, and the other is to act as a reducing agent. The solubility of the chemicals and the reduction rates in this system could be adjusted by varying the reaction temperature.[42–44] A modified process was recently reported by Xia's group[43–45] for the shape control of noble metallic nanostructures in the presence of additives such as organic surfactants, polymers, biomacromolecules, coordinating ligands, or inorganic ionic species. A typical example is the use of poly(vinylpyrrolidone) (PVP), which was also demonstrated to be a weak reducing agemt recently in addition to a conventional stabilizer.[45,46] An elaborated polyol process was introduced to the preparation of sub-micrometer zinc oxide.[47] Other functional metal oxide nanomaterials including binary and ternary oxides, as well as metal sulfides have also been obtained by the diethylene glycol mediated process adopted by Feldman and collaborators.[48–51] Bulk lead sulfide is a direct semiconductor with narrow band gap ($E_g = 0.41$ eV) and has a rather large excitation Bohr radius of 18 nm. If made into nanoclusters with a diameter of less than its Bohr radius, together with large electron and hole Bohr radius, large confinement energies of this semiconductor could be

(32) Seo, D.; Park, J. C.; Song, H. *J. Am. Chem. Soc.* **2006**, *128*, 14863–14870.
(33) Zhang, J.; Gao, Y.; Alvarez-Puebla, R. A.; Buriak, J. M.; Fenniri, H. *Adv. Mater.* **2006**, *18*, 3233–3237.
(34) Kim, F.; Connor, S.; Song, H.; Kuykendall, T.; Yang, P. D. *Angew. Chem., Int. Ed.* **2004**, *43*, 3673–3677.
(35) Gou, L. F.; Murphy, C. J. *Nano Lett.* **2003**, *3*, 231–234.
(36) Gou, L. F.; Murphy, C. J. *J. Mater. Chem.* **2004**, *14*, 735–738.
(37) Cao, H. L.; Qian, X. F.; Wang, C.; Ma, X. D.; Yin, J.; Zhu, Z. K. *J. Am. Chem. Soc.* **2005**, *127*, 16024–16025.
(38) Houtepen, A. J.; Koole, R.; Vanmaekelbergh, D.; Meeldijk, J.; Hickey, S. G. *J. Am. Chem. Soc.* **2006**, *128*, 6792–6793.
(39) Lu, W.; Fang, J.; Stokes, K. L.; Lin, J. *J. Am. Chem. Soc.* **2004**, *126*, 11798–11799.
(40) Mokari, T.; Zhang, M.; Yang, P. *J. Am. Chem. Soc.* **2007**, *129*, 9864–9865.
(41) Zhang, K. Q. *Nature* **2004**, *429*, 739–743.
(42) Fiévet, F.; Lagier, J. P.; Figlarz, M. *MRS Bull.* **1989**, *14*, 12–29.
(43) Wiley, B.; Sun, Y. G.; Mayers, B.; Xia, Y. N. *Chem. Eur. J.* **2005**, *11*, 454–463.
(44) Toneguzzo, P.; Viau, G.; Acher, O.; Fievet-Vincent, F.; Fievet, F. *Adv. Mater.* **1998**, *10*, 1032–1035.
(45) Xiong, Y. J.; Washio, I.; Chen, J. Y.; Cai, H. G.; Li, Z. Y.; Xia, Y. N. *Langmuir* **2006**, *22*, 8563–8570.
(46) Hoppe, C. E.; Lazzari, M.; Pardinas-Blanco, I.; Lopez-Quintela, M. A. *Langmuir* **2006**, *22*, 7027–7034.
(47) Jezequel, D.; Guenot, J.; Jouini, N.; Fievet, F. *J. Mater. Res.* **1995**, *10*, 77–83.
(48) Feldmann, C. *Adv. Mater.* **2001**, *13*, 1301–1303.
(49) Feldmann, C. *Adv. Funct. Mater.* **2003**, *13*, 101–107.
(50) Feldmann, C.; Jungk, H. O. *Angew. Chem., Int. Ed.* **2001**, *40*, 359–362.
(51) Feldmann, C.; Metzmacher, C. *J. Mater. Chem.* **2001**, *11*, 2603–2606.

envisioned.[52] These, coupled with its exceptional third-order nonlinear optical properties, render PbS nanomaterial potential applications in electroluminescent devices such as light-emitting diodes and optical devices such as optical switches.[53] Therefore intensive efforts have been made on the synthesis of nanoscale PbS materials. Various approaches have been reported, including confined synthesis within hosts such as micelles, polymer matrix and glasses,[54–59] surface capping by organic thiolates or polymers,[53,60,61] and high-temperature refluxing approaches using surfactants as protecting ligands.[62–64] Meanwhile, 1D nanorods and nanowires[65–69] and star-shaped PbS nanostructures[24,70–74] have been pursued in order to explore more applications for this semiconductor.

In this work, the polyol process was employed for the synthesis of nanoscale PbS in the presence of PVP as an additive, and the size distribution of the final product was reduced by slow and constant addition of the source materials using a peristaltic pump. Nanostructured PbS of different morphology were obtained, which were found to exhibit different susceptibility of laser-induced degradation as shown by Raman spectroscopy.

Experimental Section

Synthesis of PbS Nanoparticles. All chemicals were used as received. In a typical synthesis for cubic PbS, 6.0 mL of solution of poly(vinyl pyrrolidone) (PVP-K30, 2.0 mol L^{-1} in terms of repeating unit, $M_w \approx 50000$, Shanghai Lite Chemical Technology Co., Ltd.) dissolved into anhydrous ethylene glycol (EG, Shanghai Chemical Reagents Co.) was added into a 50.0 mL three-neck flask containing a Teflon-coated magnetic stirring bar, which was connected with a reflux condenser. The solution was placed on a heating plate and heated to 160 °C under stirring until clear solution was formed. Then 0.379 g of lead(II) acetate trihydrate ($Pb(Ac)_2 \cdot 3H_2O$) and 0.095 g of thiourea (both from Shanghai Chemical Reagents Co.) dissolved into 2.0 mL of EG separately were transferred into the PVP solution using a two-channel peristaltic pump (HL-2D, Qingpu Huxi Instrument Factory, Shanghai) at a rate of 10.0 mL/h. The reaction system was kept at the same temperature for a further 8.0 min after the introduction of the source chemicals was finished. The product was collected through centrifugation after the reaction system was diluted with double distilled water. Then the black precipitates were washed by ethanol and water three times in order to wash out EG and PVP-K30.

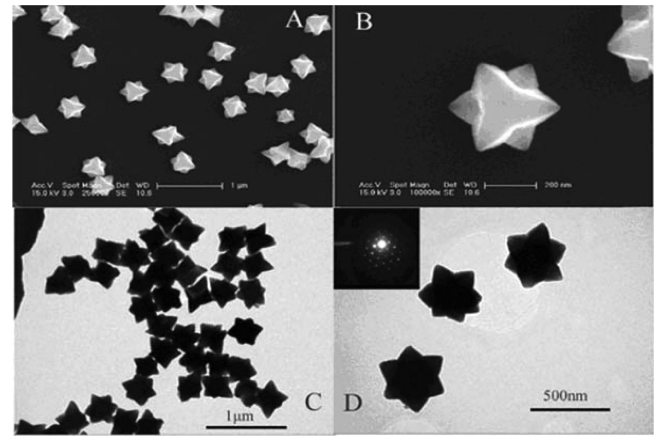

Figure 2. FESEM (A, B) and TEM (C, D) microscopy of star-shaped PbS nanoparticles. Inset in D is the ED taken near the tip of one nanoparticle.

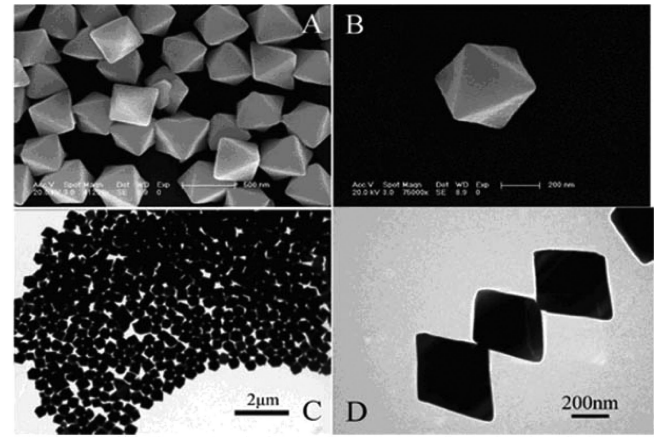

Figure 3. FESEM (A, B) and TEM (C, D) microscopy of octahedral PbS nanoparticles.

For other morphologies of nanostructured PbS, a similar synthetic procedure was deployed except the kinetic parameters were varied, such as the category of PVP (K17, $M_w \approx 8000$; K90, $M_w \approx 1300000$), the concentration of source chemicals, and the reaction temperatures.

Characterization. X-ray diffraction (XRD) of the samples was recorded with a Rigaku-Dmax2500 diffractometer using Cu Kα radiation (40.0 kV, 200.0 mA) at a step width of 8.0 deg min^{-1}. The transmission electron microscopy (TEM) images and electron

(52) Wise, F. W. *Acc. Chem. Res.* **2000**, *33*, 773–780.
(53) Patel, A. A.; Wu, F. X.; Zhang, J. Z.; Torres-Martinez, C. L.; Mehra, R. K.; Yang, Y.; Risbud, S. H. *J. Phys. Chem. B* **2000**, *104*, 11598–11605.
(54) Schneider, T.; Haase, M.; Kornowski, A.; Naused, S.; Weller, H.; Forster, S.; Antonietti, M. *Ber. Bunsen−Ges.* **1997**, *101*, 1654–1656.
(55) Lipovskii, A. A.; Yakovlev, I. E.; Kolobkova, E. V.; Petrikov, V. D. *J. Eur. Ceram. Soc.* **1999**, *19*, 865–869.
(56) Kane, R. S.; Cohen, R. E.; Silbey, R. *Chem. Mater.* **1996**, *8*, 1919–1924.
(57) Dutta, A. K.; Ho, T. T.; Zhang, L. Q.; Stroeve, P. *Chem. Mater.* **2000**, *12*, 1042–1048.
(58) Bakueva, L.; Musikhin, S.; Hines, M. A.; Chang, T. W. F.; Tzolov, M.; Scholes, G. D.; Sargent, E. H. *Appl. Phys. Lett.* **2003**, *82*, 2895–2897.
(59) Lim, W. P.; Low, H. Y.; Chin, W. S. *J.Phys. Chem. B* **2004**, *108*, 13093–13099.
(60) Chen, S. W.; Huang, K.; Stearns, J. A. *Chem. Mater.* **2000**, *12*, 540–547.
(61) Cornacchio, A. L. P.; Jones, N. D. *J. Mater. Chem.* **2006**, *16*, 1171–1177.
(62) Hines, M. A.; Scholes, G. D. *Adv. Mater.* **2003**, *15*, 1844–1849.
(63) Joo, J.; Na, H. B.; Yu, T.; Yu, J. H.; Kim, Y. W.; Wu, F. X.; Zhang, J. Z.; Hyeon, T. *J. Am. Chem. Soc.* **2003**, *125*, 11100–11105.
(64) Zhang, Z. H.; Lee, S. H.; Vittal, J. J.; Chin, W. S. *J. Phys. Chem. B* **2006**, *110*, 6649–6654.
(65) Gao, F.; Lu, Q. Y.; Liu, X. Y.; Yan, Y. S.; Zhao, D. Y. *Nano Lett.* **2001**, *1*, 743–748.
(66) Wang, S. H.; Yang, S. H. *Langmuir* **2000**, *16*, 389–397.
(67) Yu, D. B.; Wang, D. B.; Meng, Z. Y.; Lu, J.; Qian, Y. T. *J. Mater. Chem.* **2002**, *12*, 403–405.
(68) Ge, J. P.; Wang, J.; Zhang, H. X.; Wang, X.; Peng, Q.; Li, Y. D. *Chem. Eur. J.* **2005**, *11*, 1889–1894.
(69) Yong, K. T.; Sahoo, Y.; Choudhury, K. R.; Swihart, M. T.; Minter, J. R.; Prasad, P. N. *Chem. Mater.* **2006**, *18*, 5965–5972.
(70) Zhou, G. J.; Lu, M. K.; Xiu, Z. L.; Wang, S. F.; Zhang, H. P.; Zhou, Y. Y.; Wang, S. M. *J. Phys. Chem. B* **2006**, *110*, 6543–6548.
(71) Zhao, N.; Qi, L. M. *Adv. Mater.* **2006**, *18*, 359–362.
(72) Kuang, D. B.; Xu, A. W.; Fang, Y. P.; Liu, H. Q.; Frommen, C.; Fenske, D. *Adv. Mater.* **2003**, *15*, 1747–1750.
(73) Cao, H. L.; Gong, Q.; Qian, X. F.; Wang, H. L.; Zai, J. T.; Zhu, Z. K. *Cryst. Growth Des.* **2007**, *7*, 425–429.
(74) Ma, Y. R.; Qi, L. M.; Ma, J. M.; Cheng, H. M. *Cryst. Growth Des.* **2004**, *4*, 351–354.

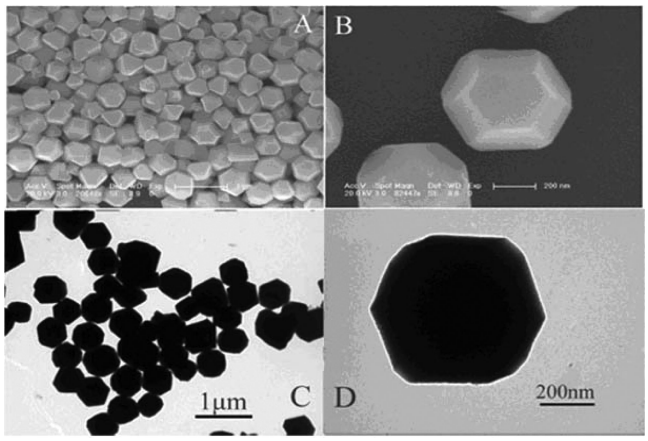

Figure 4. FESEM (A, B) and TEM (C, D) microscopy of tetradecahedral PbS nanoparticles.

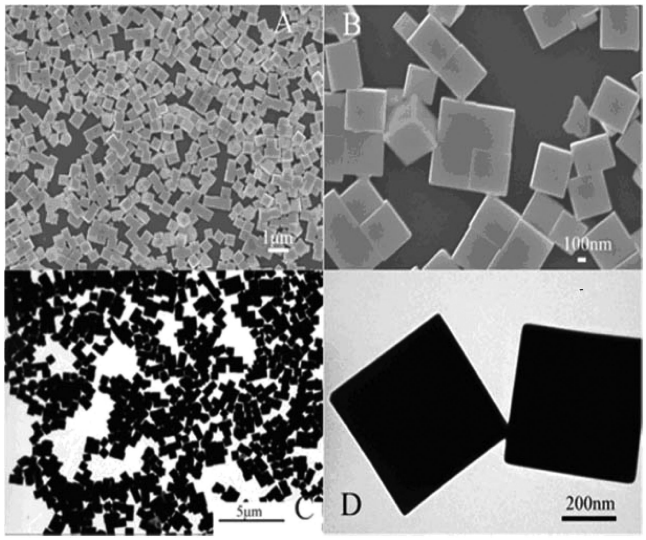

Figure 5. FESEM (A, B) and TEM (C, D) microscopy of cubic PbS nanoparticles.

diffraction patterns were taken using a JEOL microscope (1200 EX II) operated at 80.0 kV. The field emission scanning electron microscopy (FESEM) images were taken using a JSM-6700F operated at an acceleration voltage of 10.0 kV.

Spectroscopy. Ramam spectra were measured with a Renishaw 2000 model confocal microscopy Raman spectrometer with a CCD detector and a holographic notch filter (Renishaw Ltd., Gloucestershire, U.K.). Radiation of 514.5 nm was given by an air-cooled argon ion laser. All of the Raman spectra were recorded in 10.0 s.

Results and Discussion

Characterization of Typical PbS Nanostructures. Four well-defined morphologies, including star-shaped, octahedral, tetradecahedral, and cubic, of PbS with sub-micrometer size in the range of 300−500 nm have been obtained under controlled experimental conditions. Details of these conditions are summarized in Table 1. All the XRD patterns of different morphologies shown in Figure 1 are consistent with the standard JCPDS card (05-0592) except for the peak intensities, especially for (200) and (111). Compared with 1.18, the peak intensity ratio for (200) to (111) given in the JCPDS card, distinct variations for the ratios occurred for

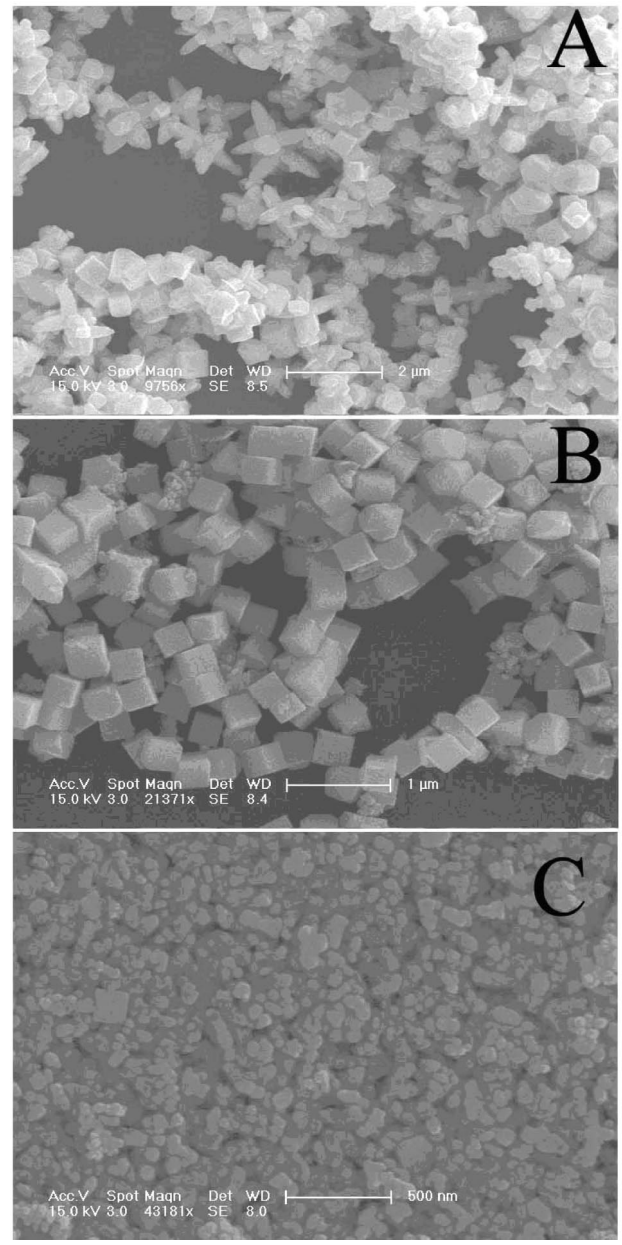

Figure 6. PbS particles with different morphologies obtained with different concentrations of PVP -K30: A, 0.0 mol/L; B, 0.5 mol/L; C, 4.0 mol/L. Concentration of $Pb(Ac)_2$: 0.5 mol/L. Mole ratio of thiourea to $Pb(Ac)_2$ (S/Pb): 1.25. Reaction temperature: 160 °C. Duration time: 8 min.

octahedral- and cube-like PbS as shown in Table 2. Such variations suggest anisotropic growth of these planes during the nanostrutures' growing processes.

Figure 2 shows both FESEM and TEM microscopies of star-shaped PbS obtained at 110 °C using 1.0 mol L^{-1} PVP-K30 as additive and with a 0.5 S/Pb ratio. This product has six symmetric branches and a narrow size distribution with the length of opposite vertexes around 300 nm. Electron diffraction (ED) shown in inset of Figure 2D was taken near one of the vertexes of one particle. The unsymmetric dots appearing in the ED might suggest that the nanoparticles are polycrystalline in nature. Figure 3 shows the microscopies of octahedral PbS. It can be seen from FESEM (Figure 3A) that most of the particles are in octahedral shape although not perfect; for example depressed triangle faces appeared

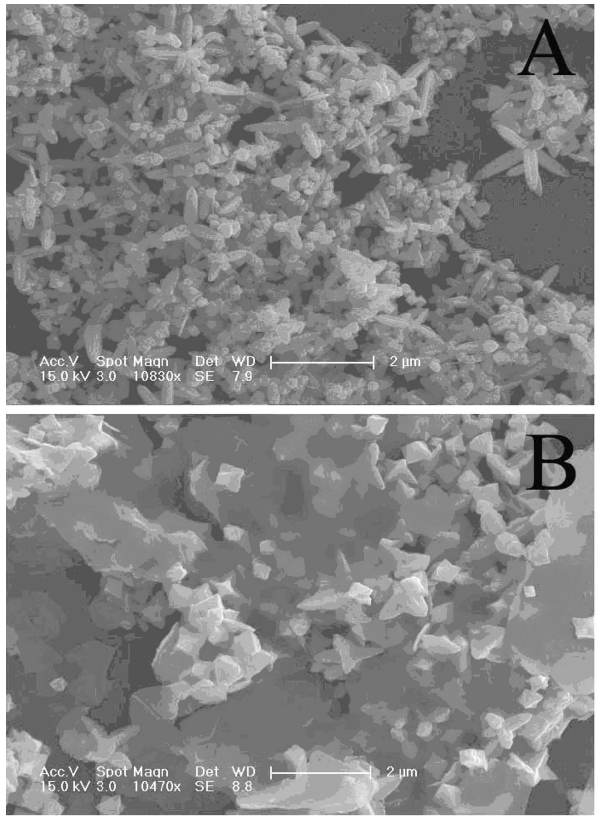

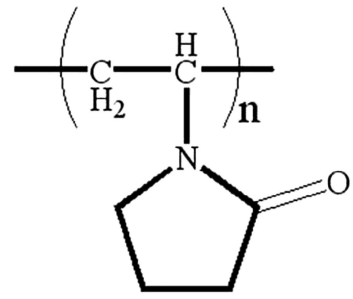

PVP-K17: 7000----------1,1000
PVP-K30: 44,000--------54,000
PVP-K90: 1,000,000--1,500,000

Figure 7. PbS obtained with the use of 2.0 mol/L PVP-K17 (A) and PVP-K90 (B). Concentration of $Pb(Ac)_2$: 0.5 mol/L. Mole ratio of thiourea to $Pb(Ac)_2$ (S/Pb): 1.25. Reaction temperature: 160 °C. Duration time: 8 min.

(Figure 3B). Compared with the star-shaped product, an increase of particle size, which is about 400 nm evaluated from opposite vertexes again (Figure 3D), could be also observed from the microscopy. Similar experimental results of tetradecahedral and cubic PbS are shown in Figures 4 and 5. The particle sizes of the two products are around 500 nm estimated from opposite square faces of individual particles.

The variation in the morphology of PbS depends on the synthetic parameters adopted in experiments. To explore the growth mechanism of PbS nanoparticles, we systematically tuned kinetic parameters, for the sake of clarity; each time only one of those deviated from the conditions for the synthesis of cubic PbS listed in Table 1, to investigate their influence on each typical morphology.

Effect of PVP. Due to the polarity of the monomer, polymeric PVP with different molecular weight can bind with polar molecules exceptionally well. They have found many commercial applications in different fields, e.g., coatings for photoquality ink-jet papers and transparencies, and ink-jet inks. Recently, PVP polymers have been extensively used in the solution-phase synthesis of colloidal particles with the most successful examples came from noble metal nanoparticles.[45] Here, they could be viewed as a steric stabilizer or capping agents, which would help to prevent the agglomeration of product. Figure 6 shows the morphologies of PbS obtained with the absence and presence of different concentrations of PVP-K30.

Without PVP, various morphologies including elongated six-pod and other irregular particles could be obtained as shown in Figure 6A. When the concentration of PVP-K30 was 0.5 mol L^{-1}, the dominated products are cubic PbS with particle size around 300 nm, together with some discrete small particles. Exclusive cubic PbS particles (Figure 4) with size of about 500 nm were synthesized with the increase of the PVP-K30 concentration to 2.0 mol L^{-1}. Further increase of its concentration to 4.0 mol L^{-1}, however, results in the formation of much smaller particles, as shown in Figure 6C. A plausible explanation to this phenomenon could be due to the increase of viscosity in the reaction system, which might cause the diffusion of ions or growing unit more difficult and suppress the anisotropic growth of PbS nanoparticles. These observations clearly show that the presence of PVP is beneficial to the control of both the morphology and grain size of the nanostructured PbS.

We also noticed that the molecular weight of PVP affected the final morphologies of PbS. Compared with the cubic structure, six-pod particles could be obtained when using the same weight of PVP-K17 and K90 as additives (Figure 7). For the former one where the molecular weight is in the range of 7000–11000, elongated six-pod particles appeared to be the major product (Figure 7A), which is akin to the absence of PVP as shown in Figure 6A and probably because of its poor steric effect as a polymeric with a short chain length. For the case of PVP-K90, the polymer itself remains in the final product even after being rinsed with copious amount of distilled water (Figure 7B). Unlike the case of using a higher concentration of PVP-K30, where the increase of viscosity causes decreases of particle size, products obtained here appear to be star-shaped with various particle sizes.

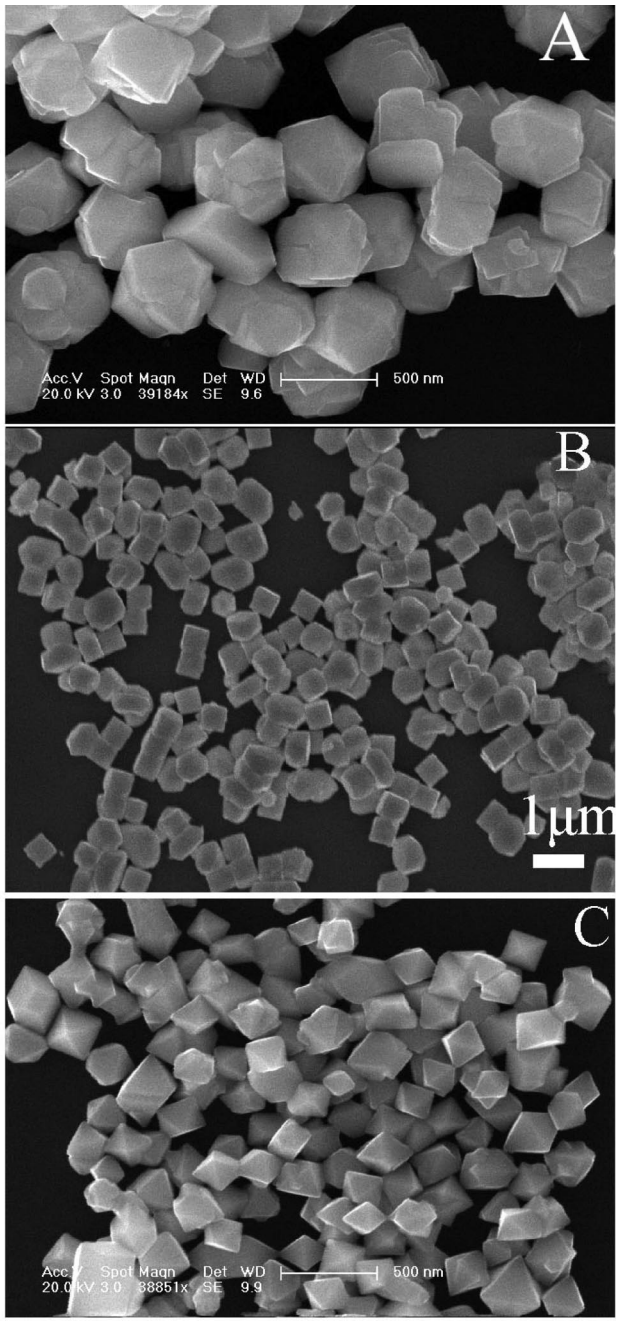

Figure 8. PbS obtained with the use of 1.0 mol/L PVP-K17 (A), PVP-K30 (B), and PVP-K90 (C). Concentration of $Pb(Ac)_2$: 0.5 mol/L. Mole ratio of thiourea to $Pb(Ac)_2$ (S/Pb): 0.8. Reaction temperature: 160 °C. Duration time: 8 min.

Further changing the concentration of all three kinds of PVP, together with lowering the mole ratio of S/P to 0.8, irregular particles were obtained using PVP-K17 as additive, while nearly cubic and octahedral PbS nanoparticles were synthesized in the system containing PVP-K30 and K90, respectively (Figure 8). Although we have observed that the presence of PVP is beneficial to the control of both morphology and grain size of nanostructured PbS, so far no direct relation could be set up between the PVP polymers and the morphology and size of the final products.

Effects of Reaction Temperature and Duration Time. The synthesis should be carried out at elevated temperature to facilitate the release of sulfur ions from thiourea in EG and initiate the reaction between the two constituent ions. At low temperature, e.g., 80 °C, only irregular nanoparticles with low yield and size less than 300 nm could be synthesized as shown in Figure 9A. Star-shaped-like particles with similar size (Figure 2) could be obtained, along with the dramatic increase of yield (>90%) and improvement of crystallinity, at 110 °C. The evolution continues as cubic products (Figure 4) with nearly 500 nm particle size was produced at 160 °C and dendritic PbS cooexisted with cubic, octahedron, and six-pod nanoparticles were yielded at 190 °C, as shown in Figure 9B. At designated reaction temperature for those typical PbS products, prolonging the reaction time longer than 8.0 min, instead of observing morphology transformations among them, all products tend to grow into larger irregular particles.

Effects of S/Pb Ratio and Sulfur Sources. The effects of the mole ratio of thiourea to $Pb(AC)_2$ could be also found in Table 1 when the reactions were carried out at 160 °C, where the morphology of PbS changed from octahedral to tetradecahedral and cubic accordingly when the S/Pb ratios gradually increased from 0.5 to 1.0 and 1.25. For comparison, when S/Pb was 0.5, the concentration of PVP was increased from 1.0 to 2.0 mol L^{-1}. Such increase did not change the octahedral morphology of PbS significantly, as shown in Figure 10A. A further increase of the ratio to 5.0 gives dendritic together with some cubic nanostructured PbS, as shown in Figure 10D. Using $Na_2S \cdot H_2O$ as a sulfur source under similar conditions, only small irregular PbS nanoparticles could be obtained.

Effect of $Pb(Ac)_2$ Concentration. Decreasing the concentration of $Pb(Ac)_2$ leads to the particle size shrinkage of cubic PbS as shown in Figure 11 when the other experimental conditions for synthesizing typical cubic PbS paricle remained unchanged. Cubic PbS nanoparticle with edge length around 110 nm were obtained when the concentration of $Pb(Ac)_2$ was 0.1 mol L^{-1}. The particle size was nearly doubled by doubling the amount of $Pb(Ac)_2$ added to the reaction system. It seems that the particle size depends linearly (Figure 11F) on the concentration of $Pb(Ac)_2$within 0.1−0.5 mol L^{-1} or even broader concentration scope in this system. Such control over the particle size of nanostructured PbS would be beneficial to the investigation of the dependence of their physical or/and chemical properties on particle size. Meanwhile, further control of particle size of other typical morphologies for nanostructured PbS might be also achieved if the kinetic factors could be favored for corresponding different concentrations of $Pb(Ac)_2$. Beyond a certain concentration scope, such a relation could not be maintained. For example, again, dendritic PbS was the major product when the concentration of $Pb(Ac)_2$ reached 1.0 mol L^{-1}, as shown in Figure 11E.

Growth Mechanism. In EG, the dissolved Pb^{2+} ion and S^{2-} ion released from thiourea at elevated temperature lead to the formation of PbS. When both constituent ions are available in the solvent, the energy barrier for forming PbS nuclei should be fairly low as can be inferred from its extremely small solubility product in aqueous solution. After forming the nuclei, the constituents will be incorporated to existing nuclei with less energy than that for nucleation. Such

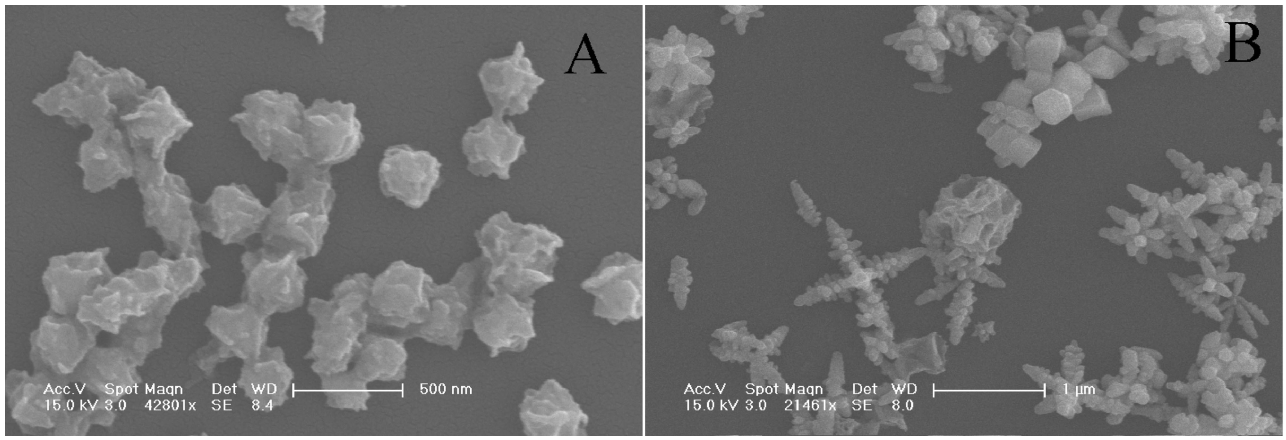

Figure 9. PbS obtained under different temperatures: 80 (A); 190 °C (B). Concentration of PVP-K30: 2.0 mol/L. Concentration of $Pb(Ac)_2$: 0.5 mol/L. Mole ratio of thiourea to $Pb(Ac)_2$ (S/Pb): 1.25. Reaction temperature: 160 °C. Duration time: 8 min.

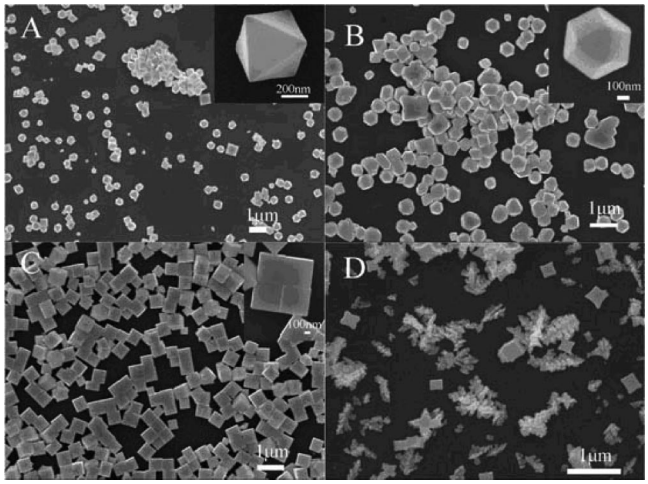

Figure 10. PbS obtained with different mole ratio of thiourea to $Pb(Ac)_2$ (S/Pb): 0.5 (A), 1.0 (B), 1.25 (C), and 5.0 (D). Concentration of $Pb(Ac)_2$: 0.5 mol/L. Concentration of PVP-K30: 2.0 mol/L. Reaction temperature: 160 °C. Duration time: 8 min.

postgrowth would be largely controlled by the kinetic parameters adopted in the reaction system and responsible for the morphology variation. Even though the intrinsic structure of PbS still plays critical roles, especially for the nucleation stage where the shape of nuclei is mainly determined by the crystalline structure of the material itself[75] in forming specific shapes. As a rock salt structure, lead sulfide has a face-centered cubic (fcc) structure where each ion resides on a separate, interpenetrating fcc lattice. The calculated reticular density order for non-interpenetrating fcc structure is {111} > {100} > {110}. Without differentiating the lead and sulfur atoms in atomic arrangement, the reticular density order for rock salt PbS is {100} > {110} > {111} as a result of interpenetration of the two separated fcc elements. On the basis of this calculation, the {111} faces would have the largest surface energy and the cube would be the thermodynamically favored morphology according to Wulff's theorem.[76]

From a kinetic point of view, in growing PbS single crystals, a qualitative model that related its growth habit and supersaturation has been established by Sunagawa in 1981.[77,78] High superaturation causes the three-dimensional growth of preformed nuclei and results in the formation of dendrite structure. Decreasing the supersaturation favors the formation of concave structure and forms thermodynamically favored cubic morphology. A similar phenomenon has been also observed in the shape control of CdSe and other nanoscale semiconductors with their smallest dimensions less than 10 nm, as reported by Peng who used the term of monomer concentration instead of supersaturation.[79–81] It should be pointed out here that such supersaturation or monomer concentration (hereafter we use supersaturation only) refers to the state during the growth stage rather than the nucleation process. At higher supersaturation, progressive nucleation would occur, and the diffusion of source materials to existing nuclei might be hindered. Thus, the postgrowth of those existing nuclei would be restrained to allow their growth to larger particles, and a large size distribution could be envisoned. Since the dimension sizes of nanostructured PbS with different shapes prepared here is in the sub-micrometer range and falls into the intermediate range between the above two cases, the accepted relation between the supersaturation and morphology might be also applicable to their formation.

For the case of the star-shaped product (Figure 2), the preferential growth on {100} faces and subsequent filling of the free space among six pods could be satisfied by the low supersaturation derived from the low reaction temperature employed in our system. Similar morphology has been obtained in previous literature.[71,82] The suppression of growth on eight {111} high-energy faces occurs due to the presence of PVP, which might interact with charged {111} faces containing either pure Pb or S atom, and therefore lowering their surface energies. The fast growth on six {100} faces leads to the shrinkage of such faces as evidenced by forming a cusp at each pod and formation of star-shaped nanostru-

(75) Jun, Y. w.; Lee, J. H.; Choi, J. s.; Cheon, J. *J. Phys. Chem. B* **2005**, *109*, 14795–14806.
(76) Wulff, G. *Z. Krystallogr.* **1991**, *34*, 449–530.
(77) Sunagawa, I. *Bull. Mineral.* **1981**, *104*, 81.
(78) Henisch, H. K. Crystals in Gels and Liesegang Rings; Cambridge University Press: Cambridge, U.K. **1988**, 84.
(79) Peng, Z. A.; Peng, X. G. *J. Am. Chem. Soc.* **2001**, *123*, 1389–1395.
(80) Peng, X. G. *Adv. Mater.* **2003**, *15*, 459–463.
(81) Zhang, Y.-H.; Guo, L.; Yin, P. G.; Zhang, R.; Zhang, Q.; Yang, S. H. *Chem. Eur. J.* **2007**, *13*, 2903–2907.
(82) Smith, G. D.; Firth, S.; Clark, R. J. H.; Cardona, M. *J. Appl. Phys.* **2002**, *92*, 4375–4380.

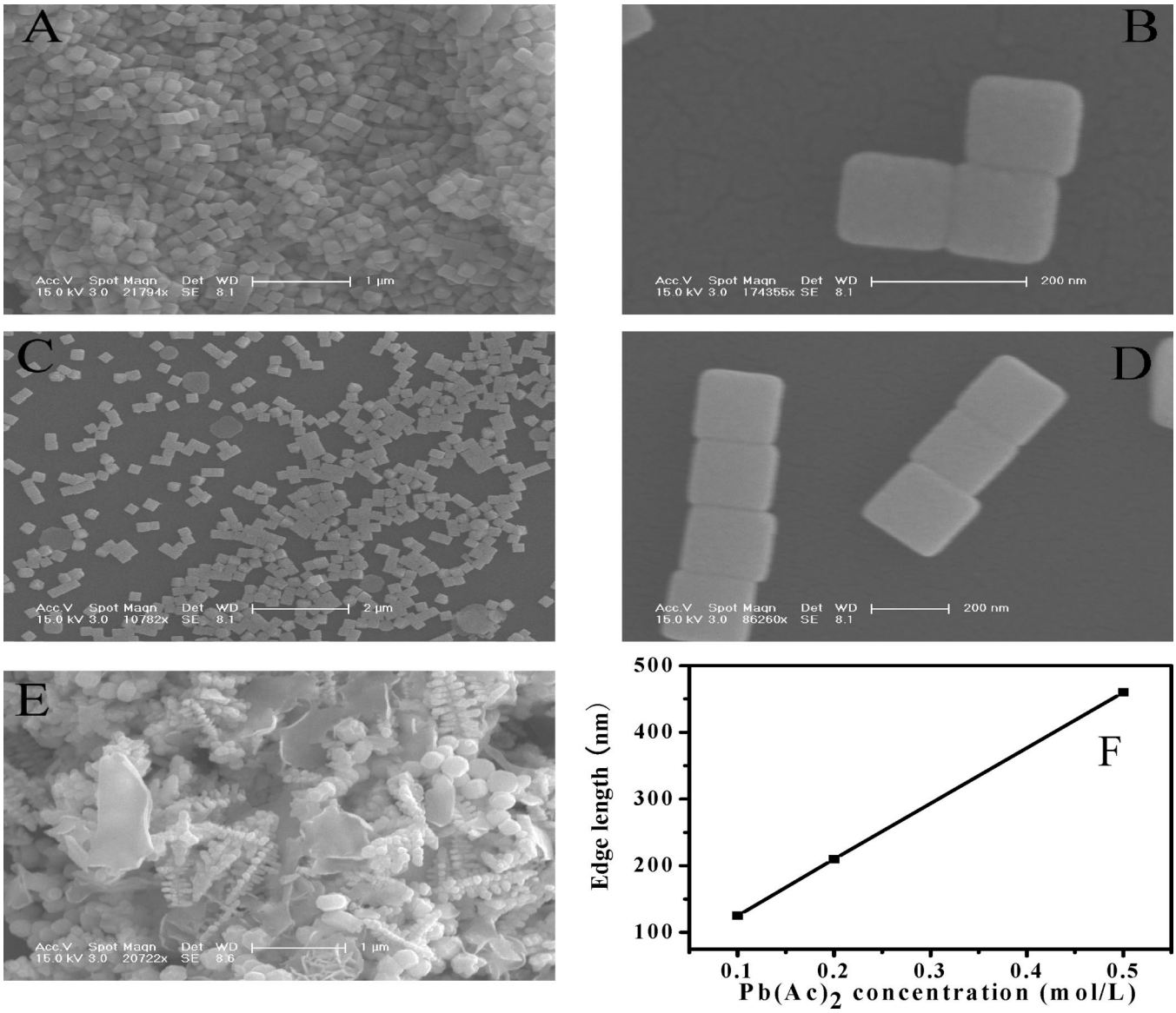

Figure 11. PbS obtained with different concentration of $Pb(Ac)_2$: 0.1 (A, B), 0.2 (C, D), and 1.0 mol/L (E). Linear relationship between edge length of cubic nanostructured PbS and concentration of $Pb(Ac)_2$ (F). Mole ratio of thiourea to $Pb(Ac)_2$ (S/Pb): 1.25. Concentration of PVP-K30: 2.0 mol/L. Reaction temperature: 160 °C. Duration time: 8.0 min.

cutre. The open spaces among the six pods are rough surfaces and have high surface energy. Such open spaces tend to be filled with constituents if the reaction could be preceded. Enhancing the supersaturation by increasing the reaction temperature, octahedral-like nanostructured PbS could be obtained. However, this is not due to the filling of open spaces among star-shaped products as the particle size increases from 300 to 400 nm. It is likely that the supersaturation might determine the growth rate ratio (R) of {100} to {111}, which could be further related to the ionic ratio of S^{2-}/Pb^{2+}. Unfortunately, the exact concentration of S^{2-} could not be obtained for the decomposition of thiourea may not be complete at the designated temperature in the reaction system. Therefore we use the mole ratio of thiourea to $Pb(Ac)_2 \cdot 3H_2O$ added as an indirect manner for our purpose under similar reaction conditions. At 160 °C, with the decrease of such a ratio from 0.5 to 1.0 and 1.25, the peak area ratio for (200) to (111) increases from 0.69 to 1.14 and 2.69 accordingly for octahedral, tetradecahedral, and cubic morphology, as given in Tables 1 and 2. The relation between the mole ratio of source materials and R would be held within a certain range. For example, when the concentration of $Pb(Ac)_2 \cdot 3H_2O$ was decreased to 0.2 and 0.1 mol L^{-1} while keeping S/Pb ratio as 1.25, cubic nanostructured PbS with an edge length of 210 and 125 nm, respectively, could be prepared (Figure 11). However, only dendritic PbS was obtained when the concentration was increased to 1.0 mol L^{-1}.

Such morphological change trend of nanostructured PbS along with supersaturation degree is reversed to that proposed by Sunagawa,[77,78] where thermodynamic cubic morphology was the major product at lower supersaturation degree. The latter case is reasonable because lower supersaturation means less reaction rate, which tends to approach the thermodynamic equilibrium stage. The different morphological change trend observed here might be attributed to the presence of the organic additive, the PVP. One thing that should be kept in mind is, this reversed trend is still tentatively effective as

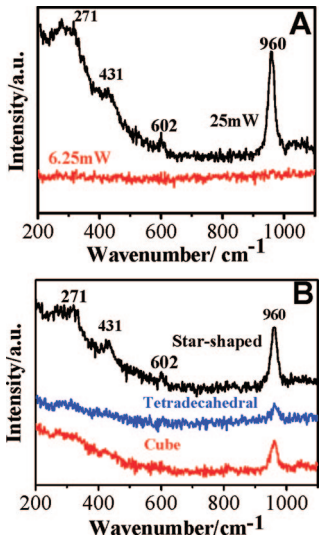

Figure 12. Raman spectra of nanostructured PbS at different laser power (A) and with different morphologies at laser power of 12.5 mW (B). Laser excitation: 514.5 nm. Irradiation time: 10.0 s.

a further increase in the supersaturation leads to the formation of dendritic nanostructure as expected.

Dendritic PbS could be obtained either under high temperature such as 190 °C (Figure 9B) or increasing the concentration of thiourea (Figure 10D) in our synthesis. A higher reaction temperature would expedite the release of sulfur ions from thiourea, while a higher concentration of thiourea would produce more sulfur ions under similar temperature. For both cases, a higher supersaturation degree was achieved by increasing the concentration of sulfur ions since the dissolved lead ions remained unchanged. When using the same concentration of Na_2S to replace thiourea as the sulfur source, an even higher supersaturation could be achieved than those through an increase of the reaction temperature or the concentration of thiourea. In this case, small irregular PbS nanoparticles were obtained under similar conditions as a result of progressive nucleation.

Using a peristaltic pump to transfer the two chemicals dissolved in EG into a flask provides another kinetic manner that might be helpful in terms of the synthetic control of nanostructured PbS. However, varying the pumping rate was proven to be similar to that by adjusting the concentrations of the two chemicals. No systematic investigations were attempted to unveil its effect on morphological changes of nanostructured PbS. Even still, this introduction of source materials, together with vigorous mechanical stirring and the presence of PVP, is beneficial for narrowing the size distributions of the four typical morphologies because the diffusions of the two ions to preformed nuclei within the solution could be kept under a constant manner.

Spectroscopic Study. Raman spectra for the four typical nanostructured PbS under various conditions are shown in Figure 12. Due to its high absorption under 514.5 nm excitation, lead sulfide is a relatively weak Raman scatterer at room temperature and susceptible to laser-induced degradation upon intense irradiation.[83] Furthermore, peak wavenumber and intensity are determined by many factors, e.g., excitation wavelength, particle size, temperature, and crystallographic facet toward irradiation. Generally, lower laser power should be applied to PbS samples in order to get discernible peaks. Even still, contradictory results for the Raman spectrum of PbS have been reported in the literature. Here we applied relatively higher power to irradiate the four typical shapes of nanostructured PbS in order to investigate their stabilities toward laser irradiation rather than the Raman spectrum of PbS itself. Under high-power irradiation, e.g., 25 mW, peaks centered around 431, 602, and 966 cm^{-1} could be clearly observed for all four samples (Figure 12A). These peaks could be attributed to the formation of lead oxysulfate such as $PbO \cdot PbSO_4$, $3PbO \cdot PbSO_4$, and $4PbO \cdot PbSO_4$ as the photooxidation products of PbS.[8283] The humplike peak centered around 270 cm^{-1} might be assigned to α-PbO after comparison with the Raman spectrum of α-PbO. When the power was decreased to 6.25 mW, no distinct peak could be found in the spectrum (Figure 12A). The absence of any peak from photooxidation products is conceivable because such low energy may not cause the degradation of nanostructured PbS. The absence of peaks from PbS was mainly due to two factors. First, the 514.5 nm laser excitation has demonstrated that the scattering efficiency of PbS could be 2 orders of magnitude smaller than that of the 632.8 nm laser excitation because the latter laser may resonant with the E_1 electronic transition of PbS (1.9 eV).[83] Another reason could be that our experiment was carried out under room temperature, which usually gives a lower signal-to-noise ratio than that at lower temperature. When 12.5 mW power was applied to these samples, as shown in Figure 12B, different peaks with varied intensity from photooxidation products of nanostructured cubic, tetradecahedron, and star-shaped PbS could be observed. An exception is for octahedral PbS, which has similar Raman spectrum obtained using 6.25 mW power. Since star-shaped PbS gives all the peaks for photooxidation products, it might be the most vulnerable morphology toward laser irradiation. Analogous analysis tells that octahedral morphology is the most stable one among the four nanostructured morphologies, while cubic and tetradecahedron locate in the intermediate position and are similar in terms of irradiation stability.

Conclusion

Star-shaped, octahedral, tetradecahedral, and cubic nanostructured PbS with narrow size distribution have been synthesized in EG solution using PVP as additive and a peristaltic pump for slowly and steadily draining the source materials into the reaction system. The supersaturation degree of free sulfur ions released from thiourea at elevated temperature determines the overall reaction rate in forming PbS and is responsible for the morphology variation. Such supersaturation degree could be adjusted by the reaction temperature as well as the concentration of thiourea in EG. With the increase of sulfur ion's supersaturation, the shape of nanostructured PbS experienced a change from star-shaped, octahedral, tetradecahedral, cubic, and dendritic structure progressively. XRD patterns of these products, through the peak area ratio change of (200) to (111), could

(83) Batonneau, Y.; Bremard, C.; Laureyns, J.; Merlin, J. C. *J. Raman Spectrosc.* **2000**, *31*, 1113–1119.

be used as an indicator for the morphological variation. Electron microscopy observations, mainly FESEM, confirmed such morphological changes. Besides shape control, it was found that the particle size of cubic PbS nanoparticles depended nearly linearly to the concentration of $Pb(Ac)_2 \cdot 3H_2O$ in the investigated range of 0.1−0.5 mol L^{-1} when the mole ratio of thiourea to $Pb(Ac)_2 \cdot 3H_2O$ (S/Pb) was kept at 1.25. Different susceptibility of laser-induced degradations for four typical morphologies has been observed under Raman spectroscopy study. It is found that octahedral nanostructured PbS is the most stable one among the four morphologies, while star-shaped PbS tends to be more vulnerable than the other three upon argon ion laser irradiation (514.5 nm) when the irradiation power was set at 12.5 mW and the irradiation time was 10.0 s.

Acknowledgment. This work was supported by the National Basic Research Program of China (Grant 2007CB925101), MOST of China (Grants 2006CB601103 and 2006DFA42610), and the National Natural Science Foundation of China (Grants 20490210, 206301040, 20602035, 20771099, and 20671087).

CM703707V